Well-balanced numerical modelling of non-uniform sediment transport in alluvial rivers

Honglu Qian[1], Zhixian Cao[2], Gareth Pender[3], Huaihan Liu[4], Peng Hu[5]

[1] PhD student, State Key Laboratory of Water Resources and Hydropower Engineering Science, Wuhan University, CHINA

[2] Professor, State Key Laboratory of Water Resources and Hydropower Engineering Science, Wuhan University, CHINA, and Professor, Institute for Infrastructure and Environment, Heriot-Watt University, UK. *Corresponding author*: e-mail: zxcao@whu.edu.cn. Phone: +86-(0)27-68774409

[3] Professor, Institute for Infrastructure and Environment, Heriot-Watt University, UK

[4] Senior Engineer, Yangtze River Waterway Bureau, Wuhan, CHINA

[5] Lecturer, School of Ocean Science and Engineering, Zhejiang University, CHINA

ABSTRACT: The last two decades have witnessed the development and application of well-balanced numerical models for shallow flows in natural rivers. However, until now there have been no such models for flows with non-uniform sediment transport. This paper presents a 1D well-balanced model to simulate flows and non-capacity transport of non-uniform sediment in alluvial rivers. The active layer formulation is adopted to resolve the change of bed sediment composition. In the framework of the finite volume SLIC (Slope LImiter Centred) scheme, a surface gradient method is incorporated to attain well-balanced solutions to the governing equations. The proposed model is tested against typical cases with irregular topography, including the refilling of dredged trenches, aggradation due to sediment overloading and flood flow due to landslide dam failure. The agreement between the computed results and measured data is encouraging. Compared to a non well-balanced model, the well-balanced model features improved performance in reproducing stage, velocity and bed deformation. It should find general applications for non-uniform sediment transport modelling in alluvial rivers, especially in mountain areas where the bed topography is mostly irregular.

Keywords: *non-uniform sediment transport; well-balanced scheme; irregular topography; shallow flow; mathematical river modelling*

1. Introduction

Since the 1990s, it has been realized that a challenge in solving the shallow water equations is to construct a well-balanced numerical scheme that satisfies the so-called *C*-property, i.e., it is capable of reproducing the exact solution for stationary flows (Bermúdez and Vázquez, 1994; Zhou et al., 2001). If a model satisfies the *C*-property, it is regarded as well-balanced (WB); otherwise it is non well-balanced (NWB).

In the last two decades, a number of well-balanced schemes have been proposed. However, most of them are applicable to the shallow water equations without sediment transport or bed deformation (Audusse et al., 2004; Aureli et al., 2008; George, 2010; Greenberg and Leroux, 1996; Liang and Marche, 2009; Rogers et al., 2003; Zhou et al., 2001). In natural rivers, the flow typically induces sediment transport and thus morphological evolution, which in turn conspire to modify the flow. The dynamics of the flow-sediment-morphology interactions is interesting in both engineering and geosciences (Simpson and Castelltort, 2006). For this reason, significant efforts have been devoted to incorporating well-balanced schemes into the modelling of sediment transport in recent years. Most of these models (Caleffi et al., 2007; Canestrelli et al., 2010; Črnjarić-Žic et al., 2004; Rosatti and Fraccarollo, 2006) are capacity models, in which sediment transport is assumed to be always equal to capacity exclusively determined by local flow and sediment conditions. As capacity models are not generally justified from physical perspectives (Cao et al., 2007), a few non-capacity WB models for sediment transport have been developed (Benkhaldoun et al., 2013; Huang et al., 2012). To date, however, almost all of the capacity or non-capacity WB models are restricted to uniform sediment transport except Huang et al. (2012). Indeed, Huang et al. (2012) proposed a non-capacity model, which was applied to predict the failure processes of natural landslide dams and the resulting floods. Yet, a rather simplified approach was used to deal with non-uniform sediment transport. In essence, the non-uniform nature of the sediment was taken into account only in estimating bed sediment entrainment flux, whilst the advection is implemented for the total sediment concentration, rather than for each sediment size fraction respectively (Huang et al., 2012).

Non-uniform sediment transport and morphological change are ubiquitous in natural rivers. For example, field observations in four mountain drainage basins in western Washington indicated a systematic downstream coarsening phenomenon in headwater channels and a subsequent shift to downstream fining (Brummer and Montgomery, 2003). Undoubtedly, it is important to be able to model non-uniform sediment transport and variation of bed sediment composition. Indeed, there has been a plethora of mathematical models for non-uniform sediment transport, including those for bed load transport (Cui et al., 1996; Hoey and Ferguson, 1994; Ribberink, 1987; Viparelli et al., 2010), suspended load (Guo and Jin, 2002; Han, 1980), and both bed load and suspended load (Armanini and Di Silvio, 1988; Wu, 2004, 2007; Wu and Wang, 2008). Unfortunately, existing models for non-uniform sediment transport are exclusively non well-balanced.

This paper presents a non-capacity WB model to simulate flows and non-uniform sediment transport in alluvial rivers. It is applicable to both bed load and suspended load transport and resolves the change of bed composition based on the active layer formulation due to Hirano (1971). To obtain well-balanced solutions, the surface gradient method (SGM) along with the finite volume SLIC scheme is employed. The SGM together with a centered discretization of the bed slope source term is very attractive for its simplicity. The reconstruction of variables and the track of wet-dry interfaces are both performed following Aureli et al. (2008). For comparison with the WB model, a NWB model based on depth gradient method (DGM) is presented. The two models are firstly applied to a static flow case to verify whether or not the *C*-property is satisfied. Then the models are tested against several cases, including the refilling of dredged trenches, aggradation due to sediment overloading and flood flow due to landslide dam failure. The results of WB and NWB models are compared and evaluated including the computing costs.

2. Mathematical Model

2.1. Governing equations

Consider one-dimensional (1D) open channel flow with rectangular cross-sections of constant width over an erodible sediment bed comprising of N size classes. Sediment feeding is also considered, whereas the fed material is assumed to enter into the water-sediment mixture flow directly (Wu and Wang, 2008). Let d_k denote the diameter of the k th size of non-uniform sediment, where the subscript $k =$ 1, 2, ...N. The model is based on the widely used three-layer structure (e.g., Cui, 2007; Hirano, 1971; Parker, 1991a, b), which consists of the bed load layer, active layer and substrate layer. Here we extend the bed load layer to sediment transport layer, in which both bed load and suspended load may exist. The active layer lies between the sediment transport layer and the substrate layer, where the sediment is assumed to be distributed uniformly in the vertical and can exchange with the upper and lower layers. The substrate layer, also known as the stratigraphy of the deposit, has certain structure in the vertical and may vary in time.

The governing equations for non-uniform sediment transport are derived from the conservation laws under the framework of shallow water hydrodynamics, including the complete mass and momentum conservation equations for the water-sediment mixture flow, the size-specific mass conservation equation for the sediments carried by the flow, the total mass conservation equation for the sediments in the bed and the size-specific mass conservation equation for the sediments in the active layer of the bed surface. In general, the complete governing equations in a SGM well-balanced conservative form are

$$\frac{\partial \eta}{\partial t}+\frac{\partial hu}{\partial x}=\frac{\Gamma}{B} \tag{1}$$

$$\begin{aligned}\frac{\partial hu}{\partial t}+\frac{\partial}{\partial x}\left[hu^2+\frac{1}{2}g(\eta^2-2\eta z)\right]=-g\eta\frac{\partial z}{\partial x}-ghS_0+\frac{u(\rho_0-\rho)\Gamma}{\rho B(1-p)}-\frac{(\rho_s-\rho_w)gh^2}{2\rho}\frac{\partial C}{\partial x}\\+u\frac{\rho_s-\rho_w}{\rho}\sum\frac{\partial hu(\beta_k-1)c_k}{\partial x}+\frac{u(\rho_0-\rho)}{\rho}\frac{E_T-D_T}{1-p}\end{aligned} \tag{2}$$

$$\frac{\partial hc_k}{\partial t}+\frac{\partial \beta_k huc_k}{\partial x}=\frac{\Gamma_k}{B}+(E_k-D_k) \tag{3}$$

$$\frac{\partial z}{\partial t}=\frac{D_T-E_T}{1-p} \tag{4}$$

$$\frac{\partial \delta f_{ak}}{\partial t}+f_{Ik}\frac{\partial \xi}{\partial x}=\frac{D_k-E_k}{1-p} \tag{5}$$

where t is the time; x is the streamwise coordinate; g is the gravitational acceleration; B is the channel width; η is the water level above the datum; z is the bed elevation (thus the flow depth $h=\eta-z$); u is the flow velocity; c_k is the size-specific sediment concentration and $C=\sum c_k$ is the total sediment concentration; Γ_k and Γ are the size-specific and total sediment feeding rates per unit channel length, $\Gamma=\sum\Gamma_k$; p is the bed sediment porosity; S_0 is the friction slope; ρ_w and ρ_s are the densities of water and sediment respectively; $\rho=\rho_w(1-C)+\rho_s C$ is the density of the water-sediment mixture; $\rho_0=\rho_w p+\rho_s(1-p)$ is the density of the saturated bed material; $\beta_k=u_{sk}/u$ is an empirical coefficient representing the velocity discrepancy between the sediment phase and water-sediment mixture flow (u_{sk} is the size-specific sediment velocity); E_k is the size-specific sediment entrainment flux and $E_T=\sum E_k$ is the total sediment entrainment flux; D_k is the size-specific sediment deposition flux and $D_T=\sum D_k$ is the total sediment deposition flux; f_{ak} is the fraction of the kth size sediment in the active layer; $\xi=z-\delta$

is the elevation of the bottom surface of the active layer; δ is the thickness of the active layer; and f_{Ik} is the fraction of the kth size sediment at the interface between the active layer and substrate layer.

For non-uniform sediment transport, the widely used active layer formulation due to Hirano (1971), Eq. (5), is adopted here to resolve the change of bed composition. According to Hoey and Ferguson (1994), $\delta = 2d_{84}$, where d_{84} is the particle size at which 84% of the sediment are finer. The complete set of the governing equations for uniform sediment transport can be easily obtained if $N = 1$ in Eqs. (1-4).

The present model is non-capacity based, which explicitly accounts for the time and space required for sediment transport to adapt to its potential capacity. This is contrary to capacity models (Caleffi et al., 2007; Canestrelli et al., 2010; Črnjarić-Žic et al., 2004; Rosatti and Fraccarollo, 2006), in which sediment concentration is presumed to be always equal to the transport capacity determined exclusively by the local flow and bed conditions, i.e., $c_k = c_{ek}$. Also, the present model is fully coupled as the interactions between the flow, sediment transport and bed evolution are explicitly incorporated in the governing Eqs. (1) and (2), and equally importantly the full set of the governing equations are numerically solved synchronously as briefed in the following.

In a NWB model, the water level η in Eqs. (1) and (2) is replaced by the water depth h, and Eqs. (6) and (7) are employed, whilst the equations related to the sediment transport and bed evolution are the same as those in the WB model, i.e., Eqs. (3-5).

$$\frac{\partial h}{\partial t} + \frac{\partial hu}{\partial x} = \frac{\Gamma}{B} + \frac{E_T - D_T}{1-p} \tag{6}$$

$$\begin{aligned} \frac{\partial hu}{\partial t} + \frac{\partial}{\partial x}\left(hu^2 + \frac{1}{2}gh^2 \right) = -gh\frac{\partial z}{\partial x} - ghS_0 + \frac{u(\rho_0 - \rho)\Gamma}{\rho B(1-p)} - \frac{(\rho_s - \rho_w)gh^2}{2\rho}\frac{\partial C}{\partial x} \\ + u\frac{\rho_s - \rho_w}{\rho}\sum \frac{\partial hu(\beta_k - 1)c_k}{\partial x} + \frac{u(\rho_0 - \rho)}{\rho}\frac{E_T - D_T}{1-p} \end{aligned} \tag{7}$$

2.2. Model closure

To close the governing equations, auxiliary relationships have to be introduced. The Manning formula is used to determine the friction slope

$$S_0 = \frac{n^2 u^2}{h^{4/3}} \tag{8}$$

where n is the Manning roughness. The bed sediment porosity p is determined using the Komura (1963) formula as modified by Wu and Wang (2006)

$$p = 0.13 + \frac{0.21}{(d_{50} \times 1000 + 0.002)^{0.21}} \tag{9}$$

with d_{50} being the median size of bed material.

The velocity discrepancy coefficient β_k is estimated by the relation due to Greimann et al. (2008)

$$\beta_k = \frac{u_*}{u} \frac{1.1(\theta_k / 0.047)^{0.17}(1 - \exp(-5\theta_k / 0.047))}{\sqrt{0.047}} \tag{10}$$

where u_* is bed shear velocity; $\theta_k = u_*^2 / (sgd_k)$ is the size-specific Shields parameter with the specific gravity of sediment $s = (\rho_s - \rho_w) / \rho_w$. Bed load sediment is usually transported at an appreciably lower velocity than the flow, so normally $\beta_k < 1$. However, for suspended sediment, the value of β_k can simply set equal to unity because suspended sediment transport has nearly the same mean velocity as the flow.

Two distinct mechanisms are involved in the sediment exchange between flow and bed, i.e., sediment entrainment due to turbulence and sediment deposition due to gravitational settling. Current understanding of the mechanisms remains far from complete and therefore the entrainment and deposition fluxes are estimated empirically by

$$E_k = \alpha_k \omega_k c_{ek} \tag{11}$$

$$D_k = \alpha_k \omega_k c_k \tag{12}$$

where ω_k is the size-specific settling velocity calculated by the formula of Zhang and Xie (1993); $\alpha_k = c_{bk}/c_k$ is an empirical parameter representing the difference between the near-bed sediment concentration c_{bk} and the depth-averaged sediment concentration c_k. Many formulas have been proposed to determine the value of α_k (Cao et al., 2011b; Guo and Jin, 1999), however, there is no evidence to show that the computed results by using any formulas are better than those by using fixed values in computational exercises. To some extent, the parameter α_k reflects the general effect of sediment transport, thus there is no need to determine each α_k for size group k. Therefore a unified parameter α is used and estimated by calibration in the simulation. The size-specific sediment concentration at capacity c_{ek} is computed as

$$c_{ek} = F_k \frac{q_k}{hu} \tag{13}$$

where q_k is the size-specific sediment transport rate at capacity regime, which is calculated by the Wu et al. (2000) formula; F_k is the areal exposure fraction of the kth sediment on the bed surface given by Parker (1991a, b) as

$$F_k = \frac{f_{ak}/\sqrt{d_k}}{\sum (f_{ak}/\sqrt{d_k})} \tag{14}$$

Wu et al. (2000) suggested that each sediment size is transported as bed load and suspended load at the same time. Therefore, the sediment transport rate of any size can be determined by

$$q_k = M_f (q_{bk} + q_{sk}) \tag{15}$$

$$\frac{q_{bk}}{\sqrt{(\rho_s/\rho_w - 1)gd_k^3}} = 0.0053\left[\left(\frac{n'}{n_b}\right)^{1.5}\frac{\tau_b}{\tau_{ck}} - 1\right]^{2.2} \tag{16a}$$

$$\frac{q_{sk}}{\sqrt{(\rho_s/\rho_w - 1)gd_k^3}} = 0.0000262\left[\left(\frac{\tau}{\tau_{ck}} - 1\right)\frac{u}{\omega_k}\right]^{1.74} \tag{16b}$$

where q_{bk} and q_{sk} are the bed load and suspended load transport rates, respectively; M_f is the modification coefficient for the Wu et al. (2000) formula, which is to be calibrated in different cases; n' is the Manning roughness corresponding to grain resistance, calculated by $n' = d_{50}^{1/6}/A$ with coefficient $A \approx 20$; n_b is the Manning roughness for channel bed; τ_b is the bed shear stress; τ is the shear stress at channel cross-section; τ_{ck} is the critical shear stress for incipient motion of bed material, estimated by $\tau_{ck} = 0.03\gamma_k(\rho_s - \rho_w)gd_k$, with γ_k being the correction factor accounting for the hiding and exposure mechanisms in non-uniform bed material (Wu et al., 2000).

The following relation is employed to evaluate the f_{Ik} (Hoey and Ferguson, 1994; Toro-Escobar et al., 1996)

$$f_{Ik} = \begin{cases} f_{sk} & \partial\xi/\partial t \le 0 \\ \phi c_k/C + (1-\phi)f_{ak} & \partial\xi/\partial t > 0 \end{cases} \tag{17a, b}$$

where f_{sk} is the fraction of the k th size sediment in the substrate layer, ϕ is the empirical weighting parameter.

2.3. Numerical solution

With regard to the well-balanced schemes for shallow water flows, Zhou et al. (2001) introduced a SGM incorporating the finite volume method with HLL Riemann solver. Equally importantly, Aureli et al. (2008) presented a weighted surface-depth gradient method

(WSDGM) under the framework of finite volume SLIC scheme. Yet, the reconstruction of flow depth in WSDGM involves a weighted average of the extrapolated values derived from SGM and DGM reconstructions. Based on the two schemes, a SGM with SLIC scheme is proposed herewith for flow and sediment transport over erodible bed. This extension is justified as the bed deformation equation [Eq. (4)] and active layer formula [Eq. (5)] are solved separately from Eqs. (1-3).

Eqs. (1-3) of the WB model constitute a hyperbolic system as real eigenvalues can be derived following a general method in the context of mathematical river modelling (Xie 1990). Thus this system can be solved by finite volume method incorporating the SLIC scheme (Toro, 2001). First, Eqs. (1-3) are written in a matrix form as

$$\frac{\partial \mathbf{U}}{\partial t} + \frac{\partial \mathbf{F}}{\partial x} = \mathbf{S}_b + \mathbf{S}_f \tag{18}$$

$$\mathbf{U} = \begin{bmatrix} \eta \\ hu \\ hc_k \end{bmatrix} \tag{19a}$$

$$\mathbf{F} = \begin{bmatrix} hu \\ hu^2 + \frac{1}{2} g(\eta^2 - 2\eta z) \\ \beta_k huc_k \end{bmatrix} \tag{19b}$$

$$\mathbf{S}_b = \begin{bmatrix} 0 \\ -g\eta \frac{\partial z}{\partial x} \\ 0 \end{bmatrix} \tag{19c}$$

$$\mathbf{S}_f = \begin{bmatrix} \Gamma/B \\ -ghS_0 + \frac{u(\rho_0 - \rho)\Gamma}{\rho B(1-p)} - \frac{(\rho_s - \rho_w)gh^2}{2\rho} \frac{\partial C}{\partial x} + \frac{u(\rho_s - \rho_w)}{\rho} \sum \frac{\partial hu(\beta_k - 1)c_k}{\partial x} - \frac{u(\rho_0 - \rho)}{\rho} \frac{E_T - D_T}{1-p} \\ \Gamma_k/B + (E_k - D_k) \end{bmatrix} \tag{19d}$$

Then an explicit finite volume discretization of Eq. (18) gives

$$\mathbf{U}_i^* = \mathbf{U}_i^m - \frac{\Delta t}{\Delta x}[\mathbf{F}_{i+1/2} - \mathbf{F}_{i-1/2}] + \Delta t \overline{\mathbf{S}}_{bi} \tag{20a}$$

$$\mathbf{U}_i^{m+1} = \mathbf{U}_i^* + \Delta t \mathbf{S}_f^{RK} \tag{20b}$$

where Δt is the time step; Δx is the spatial step; the subscript i denotes the spatial node index; the superscript m denotes the time step index; $\mathbf{F}_{i+1/2}$ and $\mathbf{F}_{i-1/2}$ represent the inter-cell numerical fluxes; $\overline{\mathbf{S}}_{bi}$ is the bed slope source term discretized with a centered difference scheme

$$\overline{\mathbf{S}}_{bi} = \begin{pmatrix} 0 \\ -g \dfrac{\overline{\eta}_{i+1/2}^L + \overline{\eta}_{i-1/2}^R}{2} \dfrac{z_{i+1} - z_{i-1}}{2\Delta x} \\ 0 \end{pmatrix} \tag{21}$$

where $\overline{\eta}_{i+1/2}^L$ and $\overline{\eta}_{i-1/2}^R$ are the evolved variables obtained from *Step 2* in the flux computation; the source term $\mathbf{S}_f^{RK}$ is computed by the second-order Runge-Kutta (R-K) method

$$\mathbf{S}_f^{RK} = \frac{1}{2}[\mathbf{S}_f(\mathbf{U}_i^{*1}) + \mathbf{S}_f(\mathbf{U}_i^{*2})] \tag{22}$$

$$\mathbf{U}_i^{*1} = \mathbf{U}_i^* \tag{23a}$$

$$\mathbf{U}_i^{*2} = \mathbf{U}_i^{*1} + \Delta t \mathbf{S}_f(\mathbf{U}_i^{*1}) \tag{23b}$$

For numerical stability, the time step satisfies the Courant–Friedrichs–Lewy (CFL) condition

$$\Delta t \le Cr \frac{\Delta x}{\lambda_{\max}} \tag{24}$$

where Cr is the Courant number and $Cr \le 1$; $\lambda_{\max}$ is the maximum celerity computed from the Jacobian matrix $\partial \mathbf{F} / \partial \mathbf{U}$. In addition, numerical tests indicate that a large source term due to friction in the momentum conservation equation, i.e., Eq. (2) in the WB model and Eq. (7) in the NWB model, may lead to numerical instability even if the CFL condition is satisfied.

Thus a stability condition for second-order R-K method for Eq. (2) and Eq. (7) is estimated (Appendix I) and imposed

$$\Delta t_s < \frac{2h^{4/3}}{gn^2 u} \tag{25}$$

where Δt_s is the time step determined by the stability condition for R-K method. When updating the solutions to the next time step, one first determines the time step Δt according to the CFL condition. Then, for each grid node (i), the maximum time step $\Delta t_s(i)$ for stability of the R-K method is calculated by Eq. (25). If $\Delta t \le \Delta t_s(i)$, Δt is directly used for the R-K method at grid i. Otherwise, the R-K method is applied consecutively for a number of sub-time steps $\Delta t_\sigma(i)$ and the summation of these sub-time steps is equal to Δt. The sub-time step $\Delta t_\sigma(i)$ is calculated by

$$\Delta t_\sigma(i) = \frac{\Delta t}{Int(\Delta t / \Delta t_s(i)) + 1} \tag{26}$$

where Int is a function indicating rounding downwards to the nearest integer. It can be readily derived from Eq. (26) that $\Delta t_\sigma(i) \le \Delta t_s(i)$, which satisfies the R-K stability condition.

The bed deformation and bed surface material composition are updated by the discretizations of Eq. (4) and Eq. (5) respectively

$$z_i^{m+1} = z_i^m + \Delta t \frac{\sum (D_k - E_k)_i^{RK}}{1-p} \tag{27}$$

$$\frac{(\delta f_{ak})_i^{m+1} - (\delta f_{ak})_i^m}{\Delta t} = \left(\frac{D_k - E_k}{1-p}\right)_i^{RK} + (f_{Ik})_i \left(\frac{\delta_i^{m+1} - \delta_i^m}{\Delta t} - \frac{\sum (D_k - E_k)_i^{RK}}{1-p}\right) \tag{28}$$

In accord with the updating of sediment concentration c_k in the flow and the fraction f_{ak} in the active layer, the composition in the substrate can be updated. Specifically, to represent its stratigraphic structure, the entire substrate is vertically divided into a number of storage layers of a prescribed thickness L_s, except the top layer, of which the thickness is $L \le L_s$. In each storage layer, the sediment is assumed to be vertically well mixed. When the bed aggrades, a new sediment layer with thickness ΔL is deposited above the antecedent substrate, as part of the active layer at a previous time becomes part of the substrate. The composition of the new sediment layer is represented by f_{Ik}, updated according to Eq. (17b). If the amount of aggradation is insufficient to increase the thickness of the top storage layer to the value L_s (i.e., $L + \Delta L \le L_s$), then the composition of the top storage layer is updated as the average of the compositions of the new sediment layer and the antecedent top layer, weighted using their respective thicknesses. If the amount of aggradation is sufficiently large to create a new storage layer ($L + \Delta L > L_s$), then the composition of antecedent top layer (immediately below the new top layer) is updated by the thickness-weighted average of those of the new and antecedent sediment, while the composition of the newly created storage layer is f_{Ik}. On the contrary, when the bed degrades, the stratigraphy is mined and the compositions in the storage layers do not change, remaining the same as initially prescribed as represented by Eq. (17a).

The numerical fluxes $\mathbf{F}_{i+1/2}$ and $\mathbf{F}_{i-1/2}$ involved in Eq. (20a) are evaluated in the following three steps using the SGM version of the SLIC scheme.

Step 1: Data reconstruction of inter-cell variables $\mathbf{U}^L_{i+1/2}$ and $\mathbf{U}^R_{i+1/2}$ to achieve second order accuracy in space:

$$\mathbf{U}^L_{i+1/2} = \mathbf{U}^m_i + \frac{1}{2}\boldsymbol{\varphi}_{i-1/2}\left(\mathbf{U}^m_i - \mathbf{U}^m_{i-1}\right) \tag{29a}$$

$$\mathbf{U}^R_{i+1/2} = \mathbf{U}^m_{i+1} - \frac{1}{2}\boldsymbol{\varphi}_{i+1/2}\left(\mathbf{U}^m_{i+1} - \mathbf{U}^m_i\right) \tag{29b}$$

where the superscripts L and R represent the left and right sides of the cell interfaces. The vector $\boldsymbol{\varphi}$ is a slope limiter, which is a function of the ratio vector $\mathbf{r}$,

$$\boldsymbol{\varphi}_{i-1/2} = \boldsymbol{\varphi}(\mathbf{r}_{i-1/2}), \quad \boldsymbol{\varphi}_{i+1/2} = \boldsymbol{\varphi}(\mathbf{r}_{i+1/2}) \tag{30}$$

$$\mathbf{r}_{i-1/2} = \frac{\mathbf{U}_{i+1}^{m} - \mathbf{U}_{i}^{m}}{\mathbf{U}_{i}^{m} - \mathbf{U}_{i-1}^{m}}, \quad \mathbf{r}_{i+1/2} = \frac{\mathbf{U}_{i+2}^{m} - \mathbf{U}_{i+1}^{m}}{\mathbf{U}_{i+1}^{m} - \mathbf{U}_{i}^{m}} \tag{31}$$

Among several slope limiter functions (Toro, 2001), the MinBee limiter function is used for $\boldsymbol{\varphi}$. Besides, the evaluation of inter-cell water depths are obtained from the reconstructed water levels

$$h_{i+1/2}^{L} = \eta_{i+1/2}^{L} - z_{i+1/2}, \quad h_{i+1/2}^{R} = \eta_{i+1/2}^{R} - z_{i+1/2} \tag{32}$$

where the inter-cell bed elevations are estimated by a linear relation

$$z_{i+1/2}^{L} = z_{i+1/2}^{R} = z_{i+1/2} = (z_i + z_{i+1})/2 \tag{33}$$

Step 2: Evolution of inter-cell variables over a time step of $\Delta t/2$ to achieve second order accuracy in time. In order to satisfy the *C*-property when SGM is adopted, the contribution due to gravity must be included:

$$\overline{\mathbf{U}}_{i+1/2}^{L} = \mathbf{U}_{i+1/2}^{L} - \frac{\Delta t}{2\Delta x}\left[\mathbf{F}(\mathbf{U}_{i+1/2}^{L}) - \mathbf{F}(\mathbf{U}_{i-1/2}^{R})\right] + \frac{\Delta t}{2}\mathbf{S}_{bi} \tag{34a}$$

$$\overline{\mathbf{U}}_{i+1/2}^{R} = \mathbf{U}_{i+1/2}^{R} - \frac{\Delta t}{2\Delta x}\left[\mathbf{F}(\mathbf{U}_{i+3/2}^{L}) - \mathbf{F}(\mathbf{U}_{i+1/2}^{R})\right] + \frac{\Delta t}{2}\mathbf{S}_{bi+1} \tag{34b}$$

where $\mathbf{S}_{bi}$ is discretized with the centered difference scheme (21) as a function of the reconstructed variables $\eta_{i+1/2}^{L}$ and $\eta_{i-1/2}^{R}$.

Similarly, the evolution of water depths in this step are given by

$$\overline{h}_{i+1/2}^{L} = \overline{\eta}_{i+1/2}^{L} - z_{i+1/2}, \quad \overline{h}_{i+1/2}^{R} = \overline{\eta}_{i+1/2}^{R} - z_{i+1/2} \tag{35}$$

Step 3: Evaluation of numerical fluxes

The numerical inter-cell fluxes are evaluated according to the First ORder CEntered (FORCE) method (Toro, 2001) with the evolved variables $\overline{\mathbf{U}}_{i+1/2}^{L}$ and $\overline{\mathbf{U}}_{i+1/2}^{R}$

$$\mathbf{F}_{i+1/2} = \frac{1}{2}(\mathbf{F}_{i+1/2}^{LF} + \mathbf{F}_{i+1/2}^{LW}) \tag{36}$$

$$\mathbf{F}_{i+1/2}^{LF} = \frac{1}{2}\left[\mathbf{F}(\overline{\mathbf{U}}_{i+1/2}^{L}) + \mathbf{F}(\overline{\mathbf{U}}_{i+1/2}^{R})\right] + \frac{1}{2}\frac{\Delta x}{\Delta t}(\overline{\mathbf{U}}_{i+1/2}^{L} - \overline{\mathbf{U}}_{i+1/2}^{R}) \tag{37}$$

$$\mathbf{F}_{i+1/2}^{LW} = \mathbf{F}(\mathbf{U}_{i+1/2}^{LW}) \tag{38}$$

$$\mathbf{U}_{i+1/2}^{LW} = \frac{1}{2}(\overline{\mathbf{U}}_{i+1/2}^{L} + \overline{\mathbf{U}}_{i+1/2}^{R}) + \frac{1}{2}\frac{\Delta t}{\Delta x}\left[\mathbf{F}(\overline{\mathbf{U}}_{i+1/2}^{L}) - \mathbf{F}(\overline{\mathbf{U}}_{i+1/2}^{R})\right] \tag{39}$$

In order to satisfy the *C*-property, a special treatment is performed at wet-dry interfaces. If the water surface in a wet cell is lower than the bed elevation of its adjacent dry cell, then the bed elevation and water level of this dry cell are both set at the level of the water surface of the wet cell temporarily only in the flux calculation section. For example, if the cell i is wet whilst the adjacent cell $i+1$ is dry and $\eta_i < z_{i+1}$, then $\eta_{i+1} = z_{i+1} = \eta_i$ is done, and as a consequence the depth in the cell $i+1$ is still zero. The occurrence of very small water depth in numerical simulations can lead to instabilities due to the possible infinite bed resistance, especially at wet-dry interfaces. To avoid this difficulty, if the computed water depth is lower than a small threshold value (1.0×10^{-5}), then the depth, velocity and sediment concentration are all set to be zero.

A motionless steady state problem ($\eta \equiv \eta_0$, $u \equiv 0$) is considered to demonstrate the well-balanced property of the numerical scheme. When the cell i and its adjacent two cells (i-1, i+1) are all wet, one can easily obtain the values of the inter-cell variables after the reconstruction in *Step 1*:

$$\eta_{i-1/2}^{R} = \eta_{i+1/2}^{L} = \eta_{i+1/2}^{R} = \eta_{i+3/2}^{L} = \eta_0,\ u_{i-1/2}^{R} = u_{i+1/2}^{L} = u_{i+1/2}^{R} = u_{i+3/2}^{L} = 0 \tag{40}$$

Then the second evolution of the variables at the inter-cell $i+1/2$ is conducted following *Step 2*, which leads to the results of $\overline{\eta}_{i+1/2}^{L} = \overline{\eta}_{i+1/2}^{R} = \eta_0$ and also

$$\left(\bar{h}\bar{u}\right)_{i+1/2}^{L} = 0 - \frac{\Delta t}{2\Delta x}\left[\frac{1}{2}g(\eta_0^2 - 2\eta_0 z_{i+1/2}) - \frac{1}{2}g(\eta_0^2 - 2\eta_0 z_{i-1/2})\right] + \frac{\Delta t}{2}\left(-g\eta_0 \frac{z_{i+1} - z_{i-1}}{2\Delta x}\right) = 0 \quad (41)$$

$$\left(\bar{h}\bar{u}\right)_{i+1/2}^{R} = 0 - \frac{\Delta t}{2\Delta x}\left[\frac{1}{2}g(\eta_0^2 - 2\eta_0 z_{i+3/2}) - \frac{1}{2}g(\eta_0^2 - 2\eta_0 z_{i+1/2})\right] + \frac{\Delta t}{2}\left(-g\eta_0 \frac{z_{i+2} - z_{i}}{2\Delta x}\right) = 0 \quad (42)$$

(i.e., $\bar{u}_{i+1/2}^{L} = \bar{u}_{i+1/2}^{R} = 0$).

Therefore, the first two components of the flux at the inter-cell $i+1/2$ can be calculated as

$$\mathbf{F}_{i+1/2}\left(\bar{\eta}_{i+1/2}^{L,R}, \bar{u}_{i+1/2}^{L,R}\right) = \mathbf{F}_{i+1/2}^{LF} = \mathbf{F}_{i+1/2}^{LW} = \begin{pmatrix} 0 \\ \frac{1}{2}g\left(\eta_0^2 - 2\eta_0 z_{i+1/2}\right) \end{pmatrix} \quad (43)$$

If one of the neighbours of the wet cell i, such as the cell $i+1$, is dry and $\eta_{i+1} = z_{i+1} > \eta_i$, the modification will be done as $\eta_{i+1} = z_{i+1} = \eta_i$. Then it is found that after the reconstruction in *Step 1*, the same results will be obtained as (40). In the next evolution (*Step 2*), the variables' values at the inter-cell $i+1/2$ are also kept to be the initial ones ($\bar{\eta}_{i+1/2}^{L} = \bar{\eta}_{i+1/2}^{R} = \eta_0, \bar{u}_{i+1/2}^{L} = \bar{u}_{i+1/2}^{R} = 0$). Finally, the flux at the inter-cell $i+1/2$ is determined by the Eq. (43) as well. Similar analyses can be applied to other wet and dry cases.

For the inter-cell $i-1/2$, following the above analyses, its flux can be derived in a similar way as Eq. (43), i.e.,

$$\mathbf{F}_{i-1/2}\left(\bar{\eta}_{i-1/2}^{L,R}, \bar{u}_{i-1/2}^{L,R}\right) = \mathbf{F}_{i-1/2}^{LF} = \mathbf{F}_{i-1/2}^{LW} = \begin{pmatrix} 0 \\ \frac{1}{2}g\left(\eta_0^2 - 2\eta_0 z_{i-1/2}\right) \end{pmatrix} \quad (44)$$

With the flux computation finished, the values of the water level and velocity at the next time are updated to be $\eta_i^{m+1} = \eta_0$, $u_i^{m+1} = 0$ due to Eq. 20(a, b). It follows that the steady static state is maintained at the discrete level. Alternatively, the *C*-property is accurately satisfied for both wet and dry bed applications.

As for the NWB model, its solution procedure is similar to the WB model except two aspects. Firstly, the depth in the NWB model is reconstructed directly instead of being computed from the reconstructed water level and bed elevation. Secondly, the discretizations of the bed slope source terms of the two models are different. The WB model adopts a second order centered difference discretization for the bed slope source term. However, when this is used in the NWB model, serious numerical oscillations or computational failure may arise in some cases (Cases 4 and 5, Table 1). Therefore, a forward difference discretization scheme is adopted instead. For Cases 1-3 in Table 1, both of the two discretizations are workable in the NWB model so comparisons between them are made. For convenience, the NWB model with a centered difference discretization for the bed slope source term is abbreviated as NWB-CDD, and that with a forward difference discretization is referred to as NWB-FDD.

3. Computational Case Study

To evaluate the WB model as compared with the NWB model, several cases (Table 1) involving irregular topographies are numerically revisited, including a case of static flow for testing the *C*-property, the refilling of a dredged trench due to van Rijn (1986), an extended case of trench refilling due to Armanini and Di Silvio (1988), an aggradation case due to sediment overloading (Seal et al., 1997) and flood flow due to a landslide dam failure (Cao et al., 2011a, b). These cases are summarized in Table 1. In all cases, the Manning roughness for sidewalls n_w is set to be 0.009 s/m$^{1/3}$, whilst the Manning roughness for channel cross-section n and for channel bed n_b are linked by $n=[(Bn_b^{3/2}+2hn_w^{3/2})/(B+2h)]^{2/3}$. The empirical weighting parameter ϕ, which was suggested to range between 0.61 and 0.86 as a function of sediment size (Toro-Escobar et al., 1996), is calibrated to be 0.65 for the present computational cases. The values of other common parameters are ρ_w= 1000 kg/m^3, ρ_s = 2650 kg/m^3, and g = 9.8 m^2/s. The values of α and M_f are both calibrated based on measured data. Other parameters are shown in Table 2.

Table 1. Summary of Test Cases

Case	Diameter (mm)	Models for comparison	Remarks
1	n/a	WB, NWB-CDD, NWB-FDD	Static flow case
2	0.16	WB, NWB-CDD, NWB-FDD	Van Rijn (1986)
3	0.075, 0.3	WB, NWB-CDD, NWB-FDD	Armanini & Di Silvio (1988)
4	0.125 ~ 64.0	WB, NWB-FDD	Seal et al. (1997)
5	0.8, 5.0	WB, NWB-FDD	Cao et al. (2011a, b)

Table 2. List of Parameter Values

Case	Cr	Δx (m)	α	M_f
1	0.9	0.25	n/a	n/a
2	0.9	0.25	18.0	2.3
3	0.9	0.1	25.0	0.5
4	0.9	0.2	20.0	1.0
5	0.9	0.04	5.0	5.0

3.1. Case of static flow

First of all, to test whether or not the present WB model satisfies the *C*-property over irregular topography, a gentle-sided (1:10) trench with an initial depth of 0.15 m is considered. Assuming the bed is fixed and the upstream and downstream bed elevation is 0 m. At the initial time, the flow is static with a stage of 0.39 m (i.e., wet bed application). There is no water or sediment input at the inlet boundary. Fig. 1 shows the computed stages and velocities at t=1 h, from the WB, NWB-CDD and NWB-FDD models. Whilst considerable oscillations of the stage are observed for the NWB-CDD and NWB-FDD models [Fig. 1(b)], the stage computed by the WB model remains unchanged [Fig. 1(a)]. In line with this observation, nonphysical velocity is generated by the NWB-CDD and NWB-FDD models [Fig. 1(d)], whereas the velocity is well preserved to be essentially 0 m/s by the WB model [Fig. 1(c)]. If the initial stage is decreased to -0.05 m, which is lower than the upstream and downstream bed elevation (i.e., with wet-dry interfaces), the initial steady and static state is also maintained by the WB model [Fig. 2(a, c)], whilst that is not the case for the two NWB models [Fig. 2(b, d)]. These suggest that the present WB model is exactly well-balanced for cases with irregular topography irrespective of whether wet-dry interfaces are involved or not.

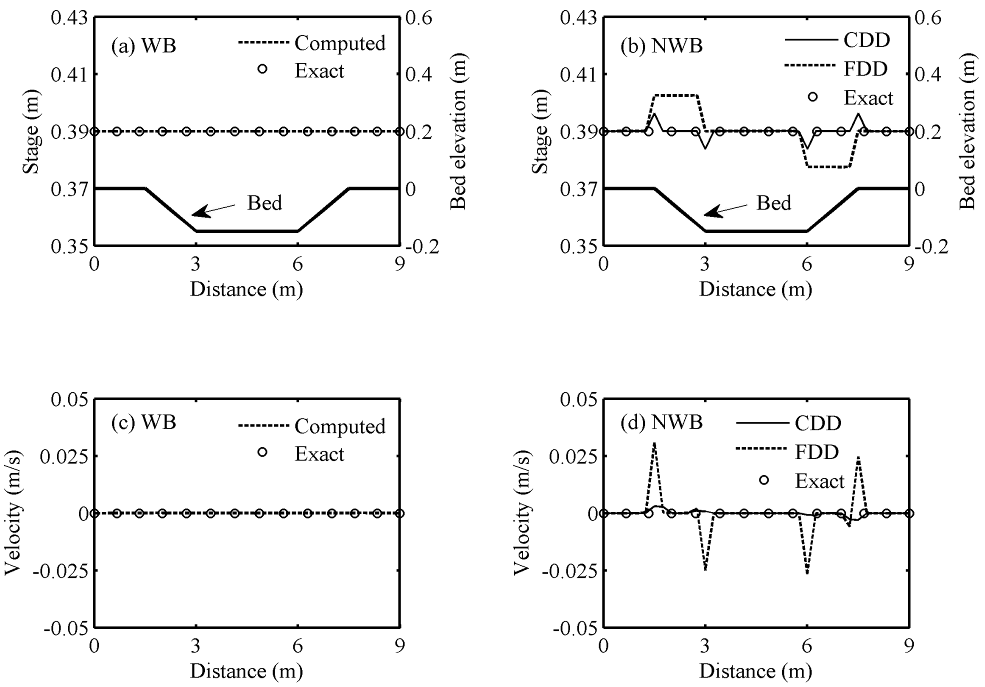

Fig. 1 Computed stages and velocities from the WB (a, c) and NWB (b, d) models in static condition at $t = 1$ h (wet bed application)

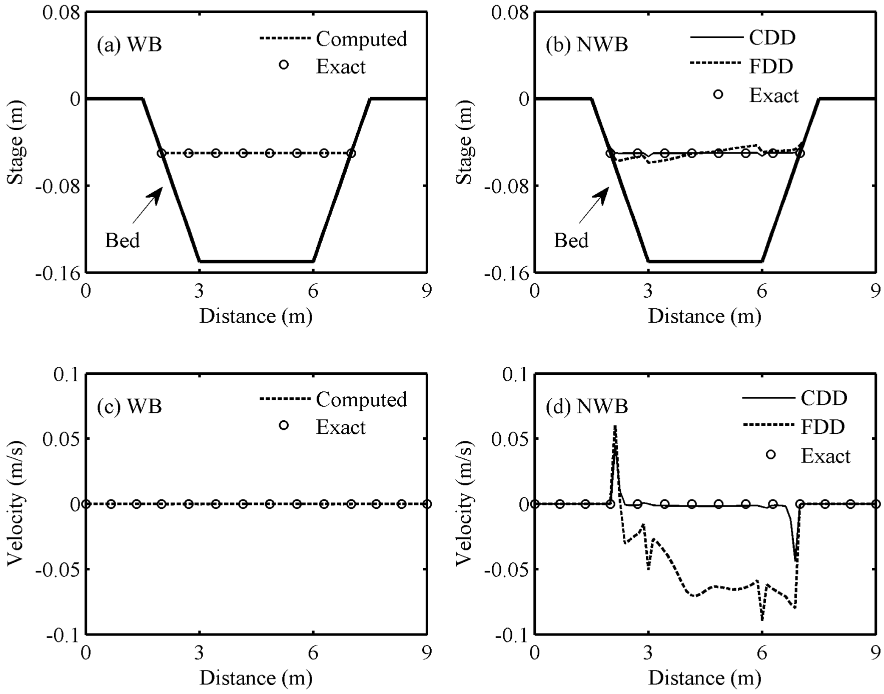

Fig. 2 Computed stages and velocities from the WB (a, c) and NWB (b, d) models in static condition at $t = 1$ h (with wet-dry interfaces)

3.2. Refilling of a dredged trench

Following the confirmation of the *C*-property, the WB and NWB models are applied to a flume experiment carried out at Delft Hydraulics Laboratory (van Rijn, 1986), which concerns the refilling of a dredged trench. A trench with the same shape as the static flow case (Case 1) was set up in a 30 m long, 0.5 m wide and 0.7 m deep flume. With a constant inflow discharge of 0.2 m^2/s, the mean flow depth and velocity at the inlet were about 0.39 m and 0.51 m/s respectively. The bed consisted of fine sand (d_{50} = 0.16 mm) and the settling velocity was about 0.013 m/s at 15℃. The Manning roughness n is approximately 0.011 s/$m^{1/3}$. During the experiment, equilibrium was maintained at the inlet boundary where the equilibrium unit-width suspended sediment rate was 0.03 kg/m/s and the sediment concentration at the cross section was 0.1508 kg/m^3.

Fig. 3 shows the stages and bed profiles computed by the WB, NWB-CDD and NWB-FDD models along with the measured bed data at t = 7.5 h and 15 h. It is noted that, for the NWB-CDD model, oscillations are significant for the stage and detectable for the bed profile, whilst the stages and bed profiles from the WB and NWB-FDD models are both smooth. Besides, the stage computed by the NWB-FDD model deviates considerably from those computed by the other two models where the bed is uneven and has steep slopes. Clearly, the WB model performs the best compared to the NWB-FDD and NWB-CDD models, agreeing well with the measured data and exhibiting no oscillations.

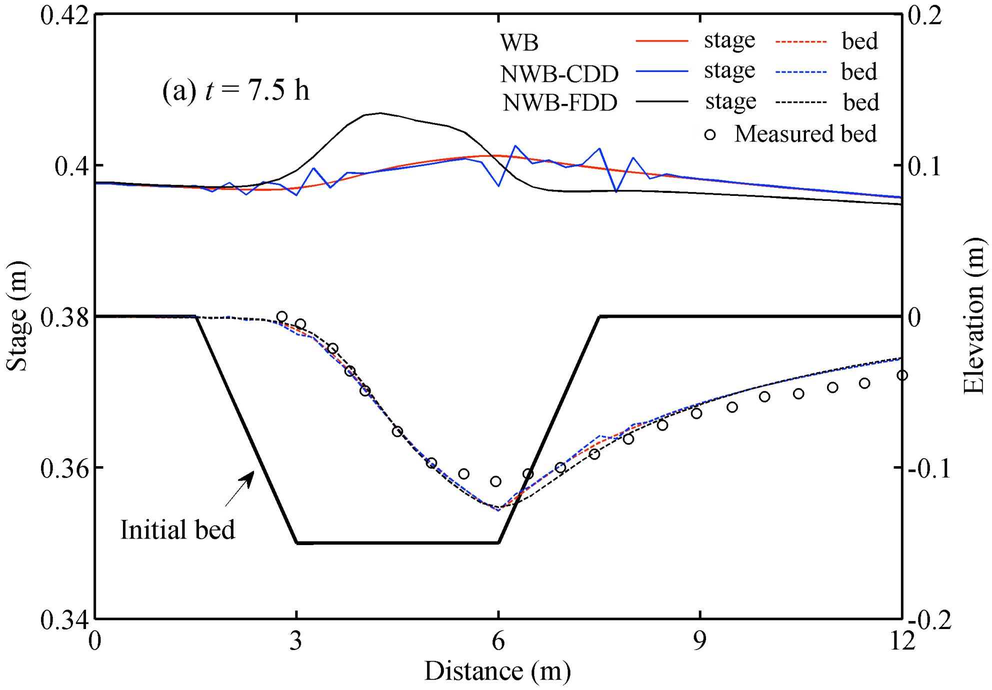

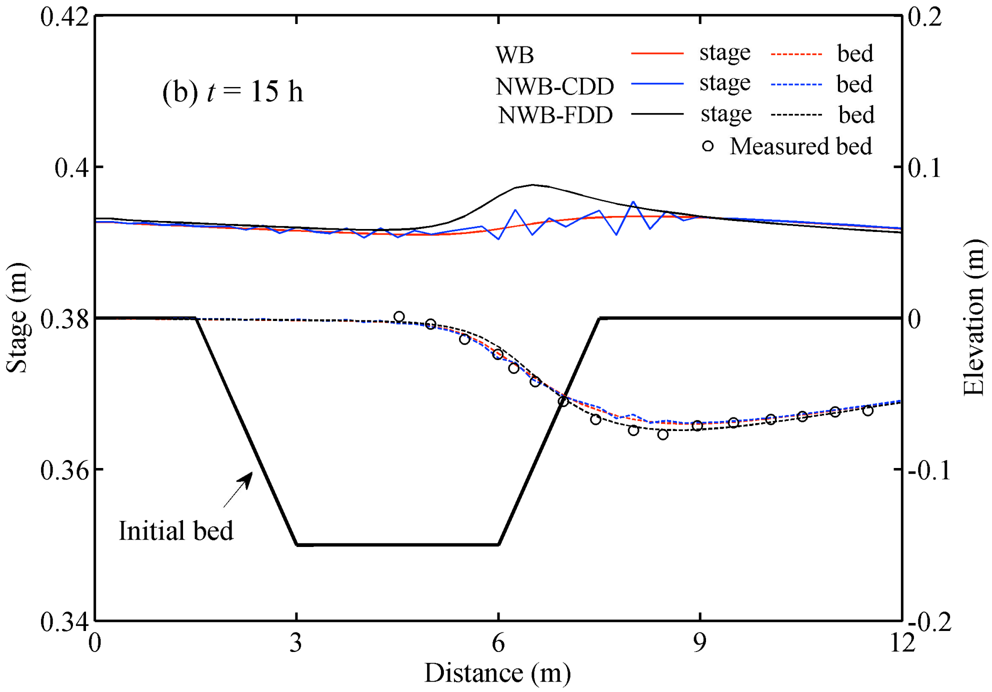

Fig. 3 Computed stages and bed profiles at (a) t = 7.5 h, and (b) t = 15 h from the WB, NWB-CDD and NWB-FDD models along with the measured data for bed

3.3. An extended case of trench refilling

In order to evaluate the ability of the WB and NWB models to simulate non-uniform sediment transport, an extended case of trench refilling due to Armanini and Di Silvio (1988) is revisited. In this case, a rather steep-sided (1:3) trench was set up and the sediment was composed of two fractions: d_1 = 0.075 mm (50%), d_2 = 0.3 mm (50%). The inflow discharge was kept constant as 0.2 m^2/s. The computed stages and bed profiles at t = 7.5 h and 15 h from the WB, NWB-CDD and NWB-FDD models are shown in Fig. 4, along with the bed profiles computed by Armanini and Di Silvio (1988). It is seen from Fig. 4 that the differences in the bed profiles are rather limited, characterizing similar performances of the present models and Armanini and Di Silvio (1988) for this particular case. And yet, similar to Fig. 3, the NWB-CDD model entails considerable oscillations in the stage and bed profile, and the NWB-FDD model entails distinct deviations in stage from the WB and NWB-CDD models. The WB model features a better performance than the NWB models in the reproducing stage and bed profiles.

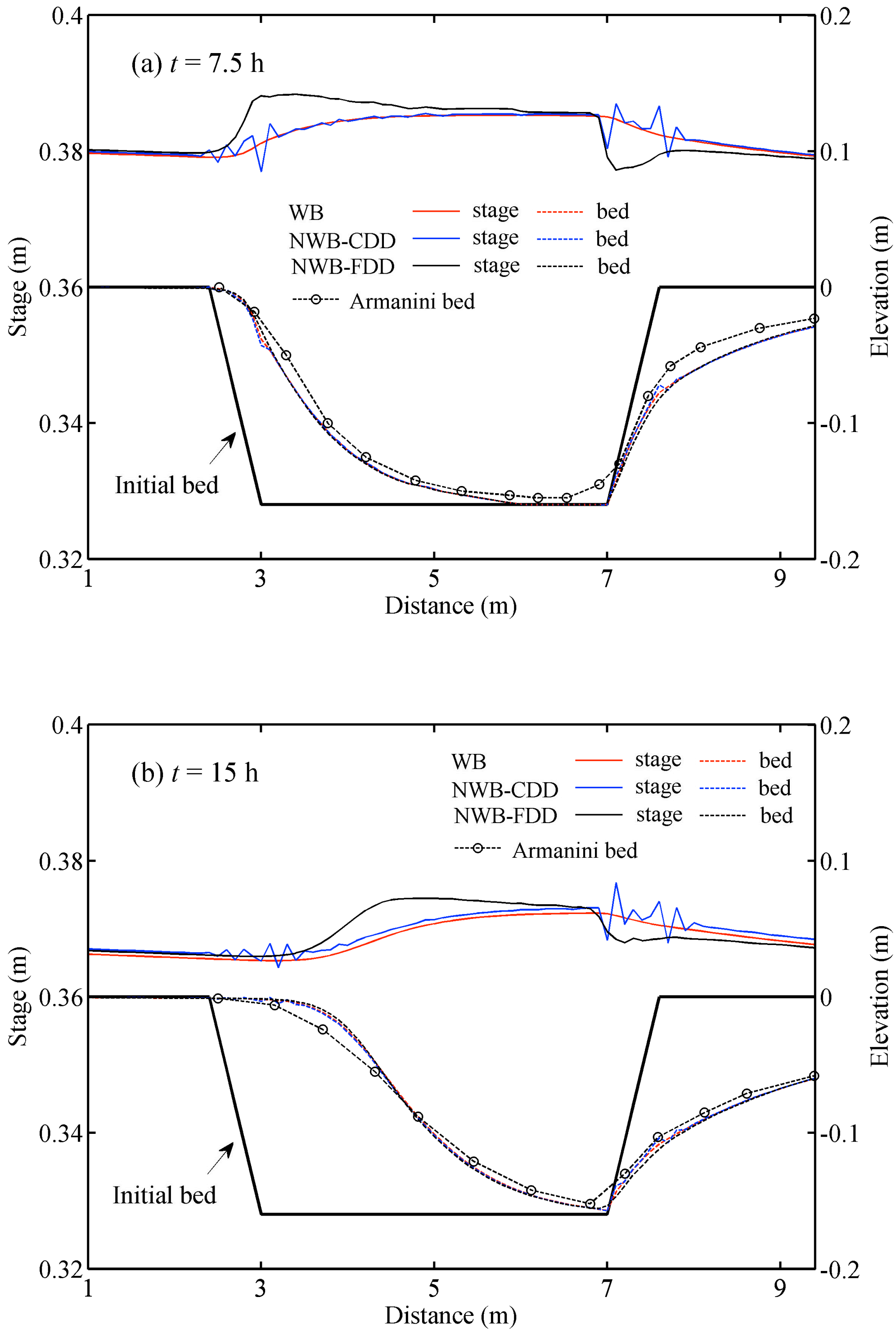

Fig. 4 Computed stages and bed profiles at (a) t = 7.5 h, and (b) t = 15 h from the WB, NWB-CDD and NWB-FDD models along with the bed profiles computed by Armanini and Di Silvio (1988)

3.4. Aggradation due to sediment overloading

Experiments of bed aggradation due to sediment overloading were performed at the St. Anthony Falls Laboratory (Seal et al., 1997). The experimental flume was 45 m long and 0.305 m wide with a slope of 0.002. At the inlet boundary, a constant clear water inflow of 0.049 m^3/s was maintained. At the outlet boundary, a tailgate was set to keep the water level at a constant. As shown in Fig. 5, sediment mixture of sizes ranging from 0.125 mm to 64 mm was fed manually at 1 m downstream of the headgate of the flume, which led to the formation of a depositional wedge. The detailed fed material composition is given in Table 3. The bed roughness $n_b = 0.027$ s/$m^{1/3}$ is estimated. The flow over the wedge was transcritical, changing from subcritical to supercritical. Three runs of experiments were conducted. Here Run 1 is selected to test the present models, in which the sediment feed rate was 11.30 kg/min, the duration of the experiment was about 16.8 hours and the tailgate water level was 0.4 m.

Table 3. Fed Material Composition

d_i (mm)	0.67	2.37	3.34	4.73	6.7	9.47	13.39	18.93	26.56	37.64	53.24	64
(%)	33.1	2.3	5.8	8.3	6.6	5.7	6.3	9.5	9.8	5.4	3.6	3.6

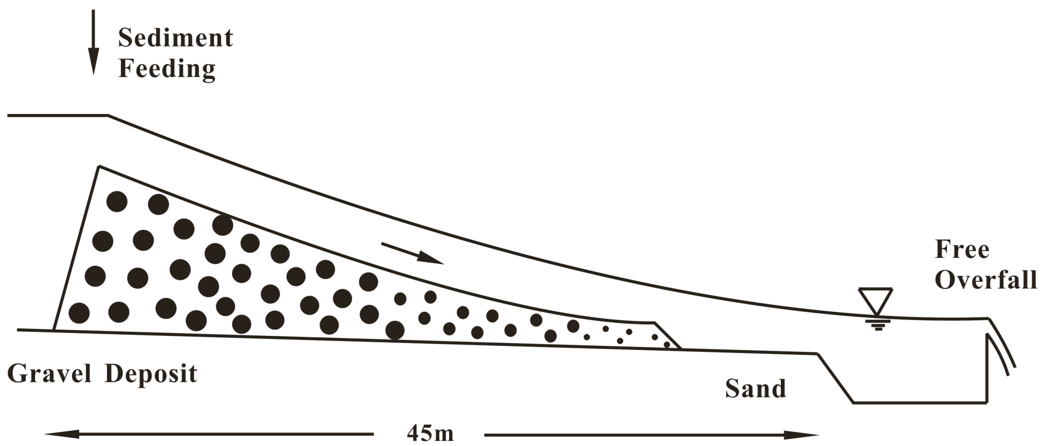

Fig. 5 Sketch of the aggradation experiments (adapted from Seal et al., 1997)

In the numerical exercises, the computational domain is extended a few meters upstream of the feeding point, and the sediment input is treated as source terms in the governing equations (Γ_k and Γ) following Wu and Wang (2008), rather than as the inflow boundary conditions (Cui et al., 1996). This is appropriate as it is hard to specify the inflow boundary conditions when the supercritical flow occurs at the inlet. Particularly, mass collapse is considered because it occurred frequently according to the observation during the experiments especially on the upstream side of the wedge because its slope was steeper than the sediment repose angle (32°).

Fig. 6 shows the measured and computed bed profiles as well as the final stages from the WB and NWB models at selected instants. As the sediment feeding proceeds, the original clear water flow becomes over-loaded, thus a wedge with rather steep leading edge and deposition front is formed and propagates downstream progressively. An undular hydraulic jump was produced at the sediment deposition front. It is seen in Fig. 6 that the bed profiles computed by the two models nearly coincide with each other except a slightly faster propagation of the wedge front from the WB model. Upstream the feeding point and downstream the wedge front, where the bed slopes are rather steep, oscillations of the stage from the NWB model are clearly spotted. Moreover, as shown in Fig. 7, the velocity from the NWB model decreases sharply around the toe of the upstream slope of the wedge, which is physically unjustifiable. In contrast, the WB model performs satisfactorily in calculating the stage and velocity profiles, without oscillations or mutations.

Interestingly, the evolution of the stratigraphy is resolved by the present models. This is characterized by the spatial and temporal distribution of grain sizes in the substrate layer. As shown in Fig. 8 from the WB model, general downstream fining at the bed surface is spotted in the longitudinal direction. Vertically, from the bed surface downwards, a coarse-to-fine structure is seen at a specific cross-section except in the immediate vicinity of the bed, where the grain size varies non-monotonically. This clearly exemplifies the very active sediment exchange between the flow and the bed, and accordingly highly complicated nature of the interactions between the flow, graded sediment transport and the evolving bed. In this regard, the results from the NWB models are qualitatively similar to those shown in Fig. 8. Quantitatively, three characteristic grain sizes (d_{10}, d_{50}, d_{90}) in substrate layer are computed and compared against the measured data (Fig. 9). Both the WB and NWB models give satisfactory reproduction of the grain sizes distribution.

To sum up, the two models are able to reasonably well resolve the non-uniform sediment transport, capture the stratigraphy evolution and characterize the variation of bed grain sizes, but the WB model is appreciably superior to the NWB models where the topography is irregular.

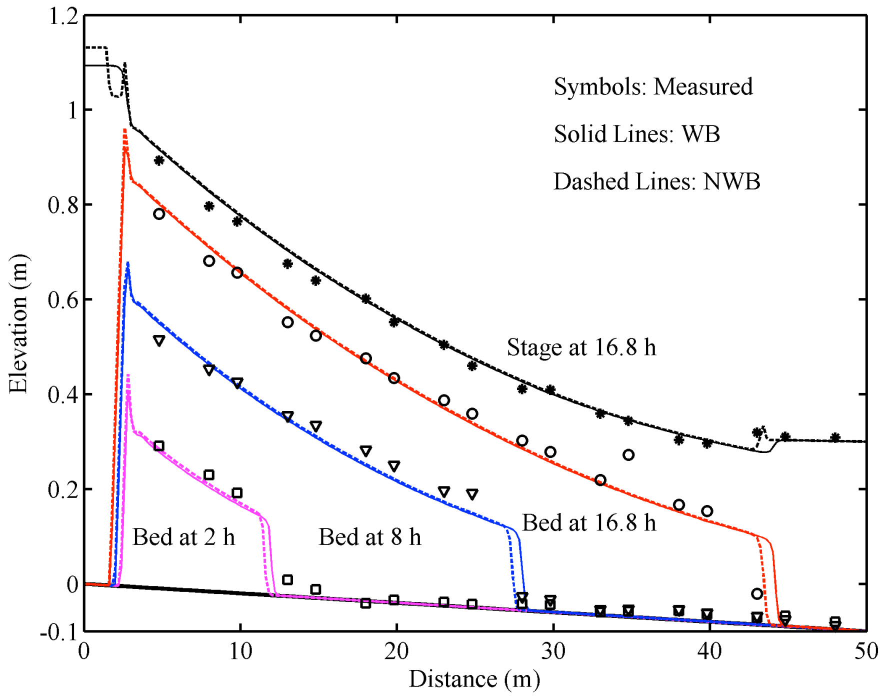

Fig. 6 Computed stages and bed profiles from the WB and NWB models against the measured

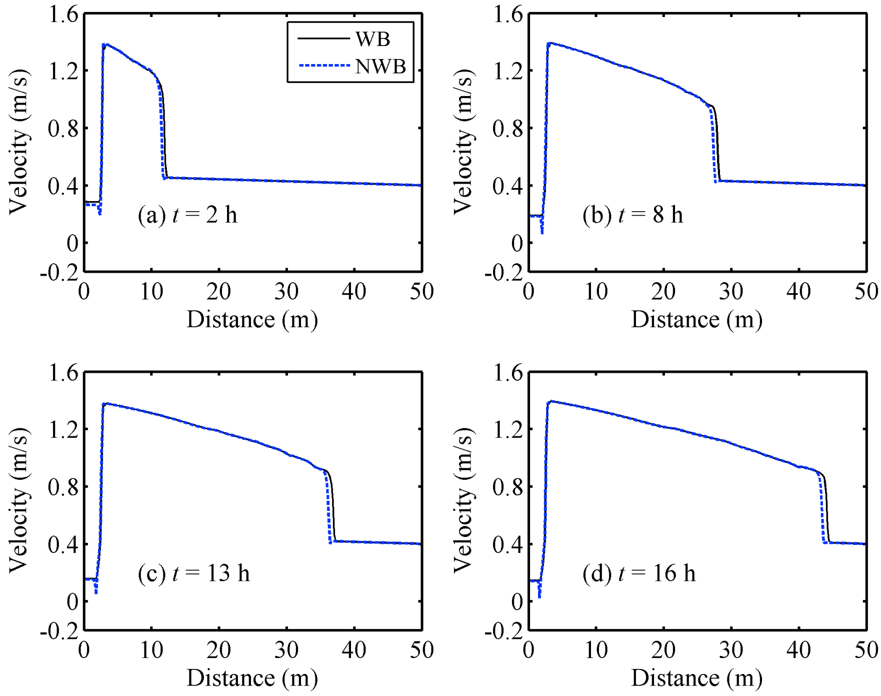

Fig. 7 Comparison between the velocity profiles from the WB and NWB model

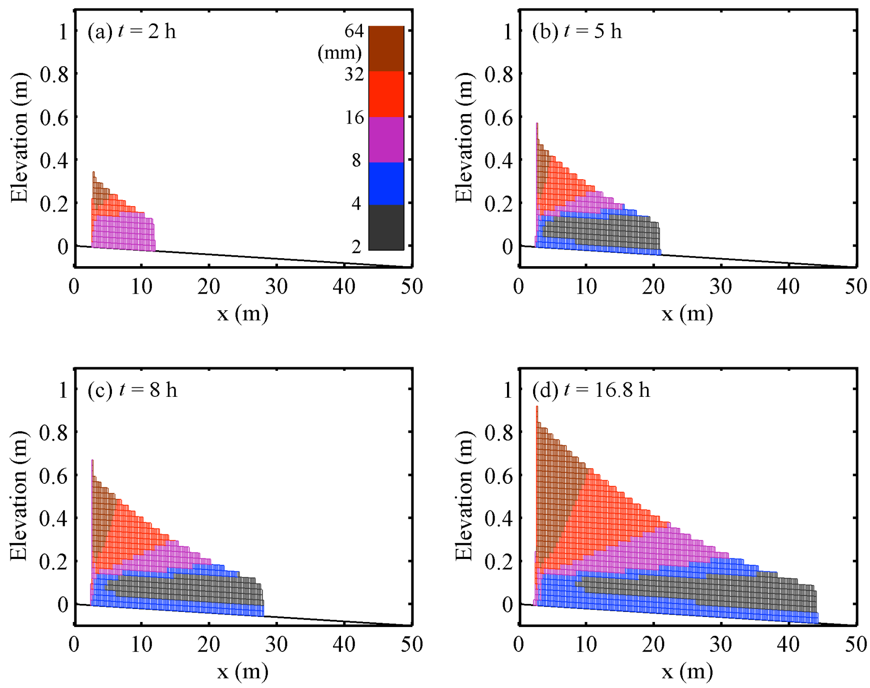

Fig. 8 Grain size distribution in substrate layer computed by WB model

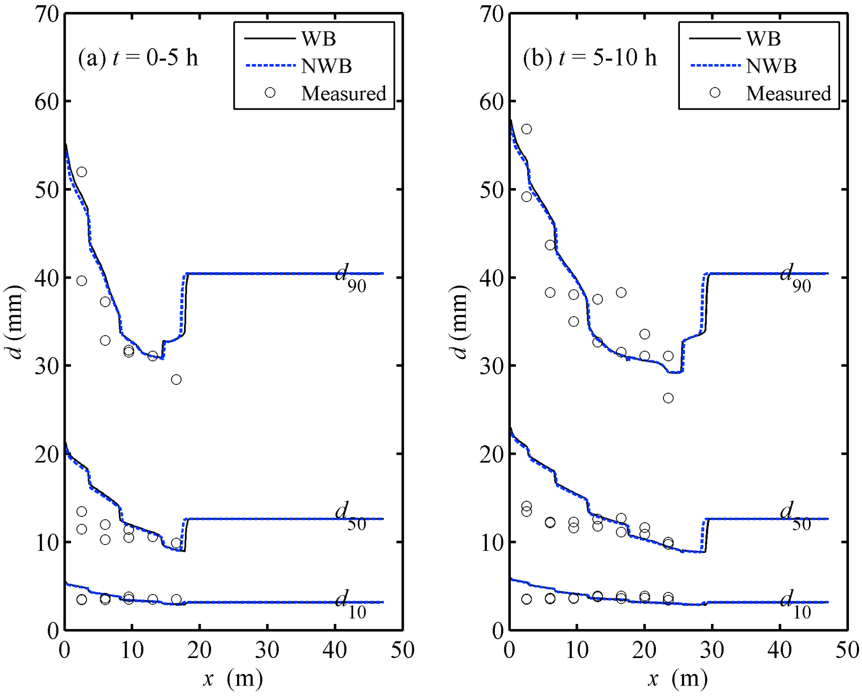

Fig. 9 Computed characteristic grain sizes in substrate layer from the WB and NWB models compared against the measured

3.5. Flood flow due to landslide dam failure

Natural landslide dams are generally composed of non-uniform sediments. However, previous mathematical modelling of landslide dam failure was almost conducted using a single median diameter (ASCE/EWRI, 2011; Cao et al., 2011b; Wang and Bowles, 2006). Recently, Huang et al. (2012) demonstrated the significant role of the non-uniform composition of natural landslide dams in dictating the breaching process and the resulting flood. Yet, they applied a simplified and compromised approach. Succinctly, the entrainment flux was estimated with respect to the local sediment size on the bed surface, whilst the advection is implemented for the total sediment concentration, rather than for each sediment fraction respectively. Here, the present WB and NWB models are evaluated as applied to the modelling of the flood due to landslide dam failure. Physically, this modelling exercise represents a step forward because for the first ever time the non-uniform nature of the sediments that comprise the landslide dams is explicitly and adequately incorporated. In contrast, a model for uniform sediment is found not to work at all as it is hard to represent the largely non-uniform composition by a single sediment size, echoing the finding of Huang et al. (2012) from a series of numerical tests on the case of the Tangjiashan landslide dam. Equally importantly, wet-dry interfaces are involved during the landslide dam failure process, thus it constitutes a prime test case to evaluate the present model in terms of well-balancing and mass conservation, in addition to shock capturing.

Cao et al. (2011a, b) documented a series of experiments on dam breach and the resulting floods in a large-scale flume of 80 m $\times$ 1.2 m $\times$ 0.8 m. The bed slope of the flume was 0.001 and the Manning roughness was approximately 0.012 s/m$^{1/3}$. Twelve automatic water-level probes were located at the center of 12 cross-sections to measure the stage hydrographs. The twelve cross-sections were 19 m, 24 m, 29 m, 34 m, 40 m, 44 m, 49 m, 54 m, 59 m, 64 m, 69 m, and 73.5 m away from the inlet of the flume respectively. Different conditions such as initial breach dimensions and dam material composition were implemented in the experiments. To demonstrate the performance of the present models, a non-uniform sediment case with no initial breach, i.e., F-case 16, is revisited here. In this case, the dam was located at the cross-section 41 m from the flume inlet, 0.4 m high and had a crest width of 0.2 m. The initial upstream and downstream slopes of the dam were 1/4 and 1/5, respectively. The inlet flow discharge was 0.025 m^3/s. The initial static water depths immediately upstream and downstream of the dam were 0.054 m and 0.048 m respectively and a 0.15-m-high weir was fixed at the outlet of the flume to hold the downstream water under the initial condition. The dam material was a mixture of the sand and gravel and the median diameter was about 2 mm. According to the gradation curves, the mixture is separated here to two size fractions: d_1 = 0.8 mm (70%), d_2 = 5 mm (30%).

As the inflow discharge is facilitated through the inlet of the flume, the water level upstream the dam gradually increases, and once the flow overtops the dam crest, dam failure commences through erosion (i.e., overtopping erosion). The wet-dry interfaces are involved during this period. In accord with the commencement of dam failure, the flow upstream the dam recedes rapidly. In contrast, the flow downstream the dam rises during the first phase and after a peak value is reached, it recedes gradually and finally attains a stable state. These processes are detailed in Cao et al. (2011a). Fig. 10 shows the stage hydrographs measured and computed by the WB and NWB models at four cross-sections: CS1 and CS5 (respectively 22 m and 1 m upstream of the dam), CS8 and CS12 (respectively 13 m and 32.5 m downstream of the dam). It is seen that the stage hydrographs computed by the WB model are in good agreement with the measured data whilst remarkable deviations are observed for the NWB model at the descending phase [Fig. 10(a, b)]. However, the computed peak stages at CS1 and CS5 from both models are discernibly higher than the measured. This is attributed to the fact that the dam subsided a little bit during the experiment, which is not taken into account in the modelling exercise. Fig. 11 illustrates the water surface and bed profiles computed by the WB and NWB models, along with the measured data for the stage. Shortly after the erosion of the dam (e.g., $t = 670$ s, 730 s), the performances of the two models are hardly distinguishable. However, the WB model matches the measured stage better than the NWB model in the later period (e.g., $t = 900$ s).

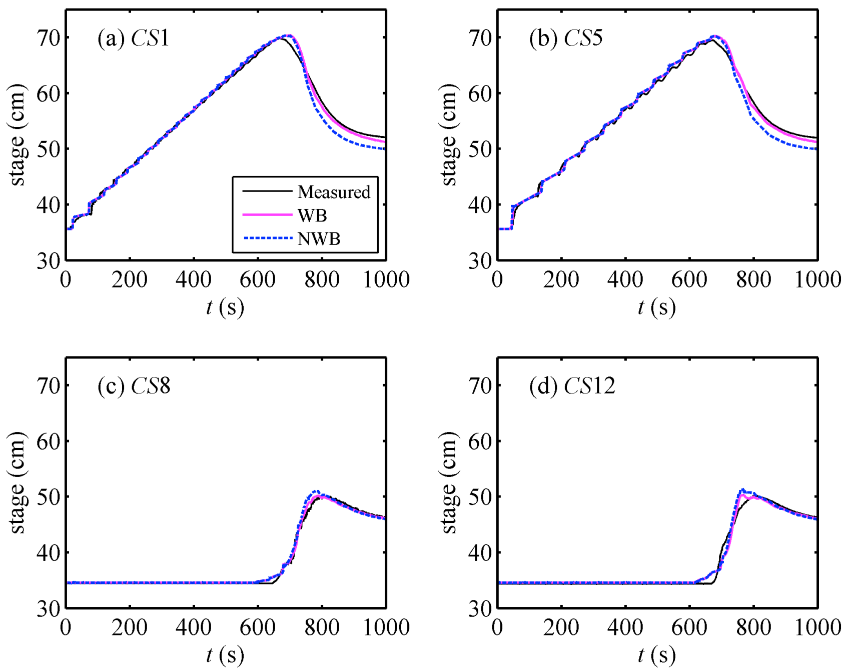

Fig. 10 Computed stage hydrographs from the WB and NWB models against the measured

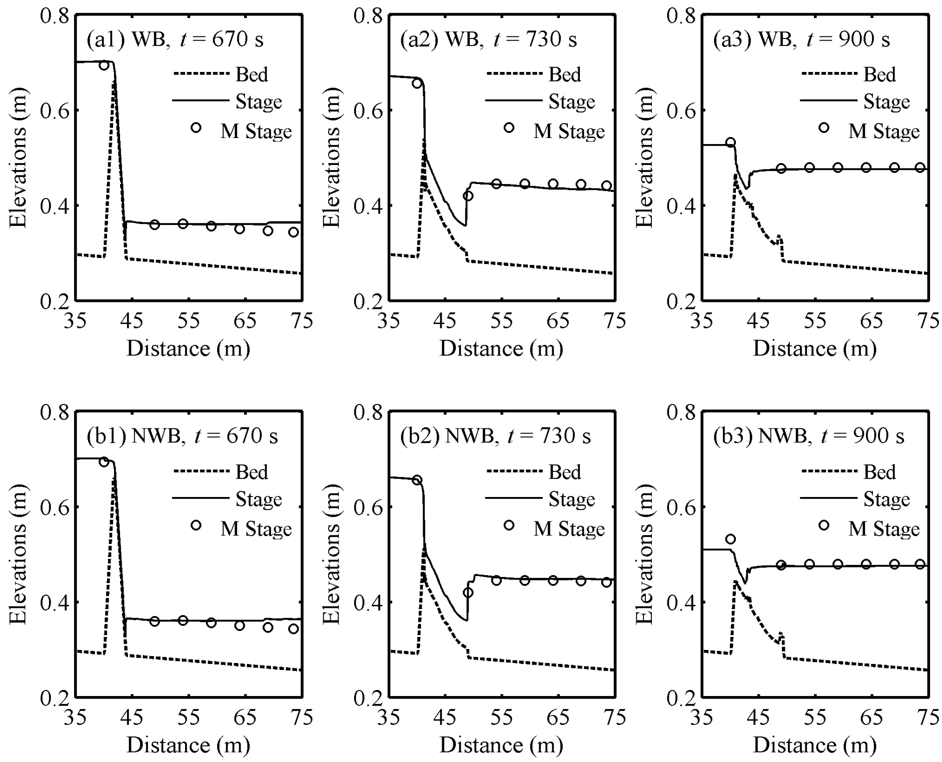

Fig. 11 Computed water surface and bed profiles from the WB (a1, a2, a3) and NWB (b1, b2, b3) models along with the measured data for stage

Fig. 12 shows the velocity profiles from the WB and NWB models at different instants. Before the flow overtops the dam (e.g., $t = 300$ s, 500 s), the velocity computed by the NWB model grows suddenly, being extremely large or small (even negative) around the toes of the dam and at the wet-dry interfaces. In addition, spurious velocity is generated in the downstream static water [Fig. 12(a, b)]. It should be pointed out that the occurrence of negative velocity does not lead to computational failure of the NWB model. This is because the friction slope [Eq. (8)], bed shear stress and Shields parameter all keep positive as determined based on u^2, which is certainly non-negative. In essence, the effects of the negative velocity due to the NWB models have been erroneously obviated numerically by using the empirical formulas of frictional slope and accordingly the bed shear stress and Shields parameter.

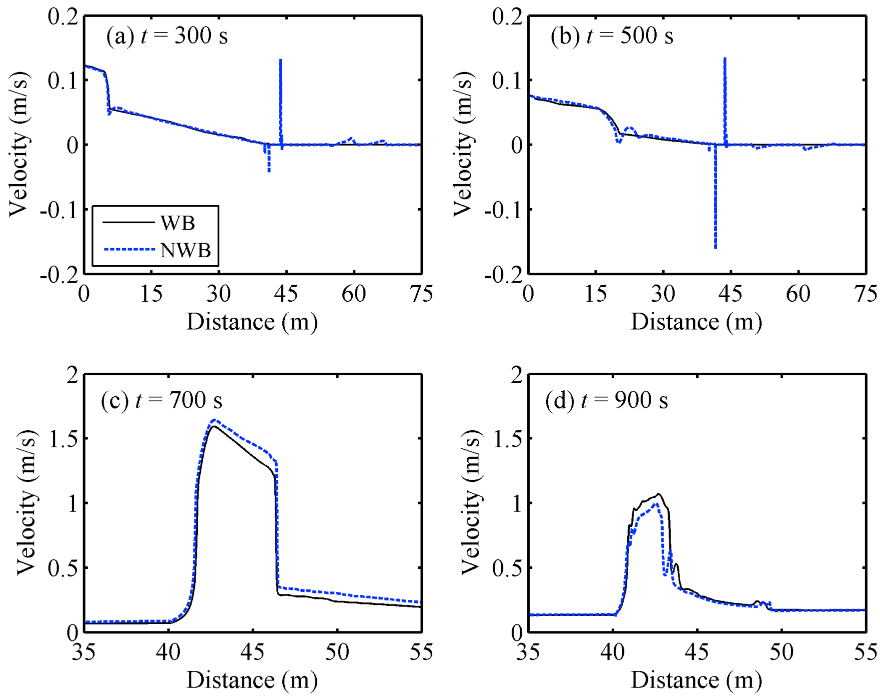

Fig. 12 Comparison between the velocity profiles from the WB and NWB models

In the context of computational river dynamics, one of the challenges is to preserve mass conservation, especially when wet-dry interfaces are involved. To evaluate the models' performance in preserving mass conservation as per the computational domain, denote the water volumes in the flow at the initial state ($t = 0$) by V_0 and at time $t > 0$ by V_t, the inflow and outflow water volumes at the up- and downstream boundaries by V_{in} and V_{out}, and the water volume from bed erosion by V_e. Then the relative error of water mass conservation is defined as $\left[V_t - \left(V_0 + V_{in} - V_{out} + V_e\right)\right]/V_t$. The relative error of sediment mass conservation can be defined similarly. If the relative errors for both water and sediment vanish, mass conservation is perfectly satisfied. In practical modelling, however, numerical errors are inevitable. For the case of landslide dam failure with wet-dry interfaces, the relative errors for water and sediment are both in the order of 10^{-4} during the computational period for both the WB and NWB models.

3.6. Discussion

The CPU time of the NWB model relative to its counterpart of the WB model is listed in Table 4. It is seen that the WB model is marginally more efficient than the NWB, but the differences are essentially negligible.

As briefed in the Introduction, the recent years have witnessed successful applications of well-balanced schemes in 2D modelling. For example, Aureli et al. (2008) presented a 2D model for shallow water flows over fixed bed under the framework of finite volume SLIC scheme, and applied it to a real field case study – the collapse of the dam on Parma river. George (2010) employed a well-balanced Riemann solver to model a 2D field case over fixed bed – the Malpasset dam-break flood (France, 1959). More closely related to the present work, Huang et al. (2012) applied a finite volume Godunov-type method incorporating the HLLC (Harten-Lax-van Leer contact wave) approximate Riemann solver to the modelling of sediment-laden floods over mobile bed, including the field case of the Tangjiashan landslide dam failure following the Wenchuan earthquake in May 2008. For applications to natural fluvial processes that generally involve non-uniform sediment transport, extending the present 1D WB model to 2D is certainly warranted. Technically, the increase in computational cost is of major concern, as a separate continuity equation for each sediment size has to be solved. In this regard, the technique of adaptive mesh refining can be incorporated, which has recently been found to be able to save computational time by an order of magnitude for modelling shallow flows and uniform sediment transport (Huang 2014).

Table 4. Relative CPU Time

Case	NWB-CDD	NWB-FDD	Remarks
1	1.004	1.005	Wet bed application
1	1.005	1.008	With wet-dry interfaces
2	1.024	1.015	
3	1.003	1.002	
4	n/a	1.011	
5	n/a	1.027	

4. Conclusions

A 1D WB model is developed to simulate fluvial processes with non-uniform sediment transport. It is fully coupled and generally applicable, as the interactions between the flow, sediment transport and bed evolution are explicitly taken into account. Incorporating the surface gradient method (SGM) with SLIC scheme, the model preserves the *C*-property exactly in both wet and dry bed applications. Its performance is demonstrated in comparison with a NWB model as applied to typical cases with irregular and erodible topography. The computed results from the present WB model agree with the measured data quite well and the model features improved performance over the NWB model that may generate unreasonable velocity or oscillations in stage and bed profiles. Inevitably, the model bears uncertainty arising from the empirical relationships introduced to close the governing equations. Extending to 2D is warranted for applications to natural fluvial processes.

Acknowledgements

This work is funded by Natural Science Foundation of China under Grant Nos. 11172217 and 11432015.

Appendix I

Consider the linear ordinary differential equation (ODE)

$$\frac{d}{dt}\psi = \lambda\psi \tag{45}$$

where λ is negative. Denoting the time step by Δt_s, the stability region for the second-order R-K method is (Cartwright and Piro, 1992)

$$\left|1 + \Delta t_s \lambda + 0.5(\Delta t_s \lambda)^2\right| < 1 \tag{46}$$

By solving Eq. (46), the stability condition is obtained

$$0 < \Delta t_s < -2/\lambda \tag{47}$$

In the momentum conservation equation, i.e., Eq. (2) in the WB model and Eq. (7) in the NWB model, the friction term generally dominates over other source terms. Thus an ODE constituted by the friction source term can be written as follows

$$\frac{d(hu)}{dt} = \lambda hu \tag{48}$$

where $\lambda = -gn^2(hu)/h^{7/3}$ is computed using the state variables at the previous time step so that Eq. (48) is linearized. Following Eq. (47), the time step ensuring stability of the second-order R-K method for Eq. (48) is

$$\Delta t_s < \frac{2h^{4/3}}{gn^2 u} \tag{49}$$

Although some source terms related to sediment in the momentum conservation equation are ignored in deriving Eq. (49), it is found through a series of numerical tests that Eq. (49) is generally applicable when those source terms are taken into account in actual modelling.

Nomenclature

A = coefficient

B = channel width

C = total sediment concentration

c_{bk} = size-specific near-bed sediment concentration

c_{ek} = size-specific sediment concentration at capacity

c_k = size-specific sediment concentration

Cr = Courant number

d_k = sediment diameter of k th size

d_{50} = median size of bed material

d_{84} = particle size at which 84% of the sediment are finer

E_k, D_k = size-specific sediment entrainment and deposition fluxes respectively

E_T, D_T = total sediment entrainment and deposition fluxes respectively

$\mathbf{F}$ = flux vector

$\mathbf{F}_{i+1/2}$, $\mathbf{F}_{i-1/2}$ = inter-cell numerical fluxes

F_k = areal exposure fraction of the k th size sediment on the bed surface

f_{ak} = fraction of the k th size sediment in active layer

f_{Ik} = fraction of the k th size sediment in the interface between the active layer and substrate layer

f_{sk} = fraction of the k th size sediment in substrate layer

g = gravitational acceleration

h = water depth

i = spatial node index

k, j = diameter index

L = thickness of the top storage layer

L_s = thickness of each storage layer except the top layer

ΔL = thickness of new deposited sediment layer

m = time step index

M_f = modification coefficient for the Wu et al. (2000) formula

n = Manning roughness

n' = Manning roughness corresponding to grain resistance

n_b = Manning roughness for channel bed

N = total number of size classes

p = bed sediment porosity

q_k = size-specific sediment transport rate at capacity regime

$\mathbf{r}$ = ratio vector

s = specific gravity of sediment

S_0 = friction slope

$\mathbf{S}_b$, $\mathbf{S}_f$ = source vectors

t = time

u = flow velocity

u_{sk} = size-specific sediment velocity

u_* = bed shear velocity

$\mathbf{U}$ = conservative variable vector

V_0, V_t = water volumes in the flow at time $t = 0$ and $t > 0$

V_{in}, V_{out} = inflow and outflow water volumes at the up- and downstream boundaries

V_e = water volume from bed erosion

x = streamwise coordinate

z = bed elevation

α = unified empirical parameter

α_k = size-specific empirical parameter

β_k = velocity discrepancy coefficient

Γ, Γ_k = total and size-specific sediment feeding rates per unit channel length

γ_k = size-specific hiding and exposure factor

Δt = time step

Δt_s, Δt_σ = time step specified by stability condition for R-K method and sub-time step

Δx = spatial step

δ = thickness of active layer

η = water level

θ_k = size-specific Shields parameter

$\lambda_{\max}$ = maximum celerity

ξ = elevation of the bottom surface of active layer

ρ_w, ρ_s = densities of water and sediment respectively

ρ = density of water-sediment mixture

ρ_0 = density of saturated bed material

τ = shear stress at channel cross-section

τ_b = channel bed shear stress

τ_{ck} = size-specific critical shear stress

ϕ = empirical weighting parameter

φ = slope limiter; and

ω_k = size-specific sediment settling velocity.

References

Armanini, A., Di Silvio, G., 1988. A one-dimensional model for the transport of a sediment mixture in non-equilibrium conditions. Journal of Hydraulic Research 26(3), 275-292.

ASCE/EWRI (ASCE/EWRI Task Committee on Dam/Levee Breaching), 2011. Earthen embankment breaching. Journal of Hydraulic Engineering 137(12), 1549-1564.

Audusse, E., Bouchut, F., Bristeau, M.O., Klein, R., Perthame, B., 2004. A fast and stable well-balanced scheme with hydrostatic reconstruction for shallow water flows. SIAM Journal on Scientific Computing 25(6), 2050-2065.

Aureli, F., Maranzoni, A., Mignosa, P., Ziveri, C., 2008. A weighted surface-depth gradient method for the numerical integration of the 2D shallow water equations with topography. Advances in Water Resources 31(7), 962-974.

Benkhaldoun, F., Elmahi, I., Sari, S., Seaid, M., 2013. An unstructured finite-volume method for coupled models of suspended sediment and bed load transport in shallow-water flows. International Journal for Numerical Methods in Fluids 72(9), 967-993.

Bermúdez, A., Vázquez, M.E., 1994. Upwind methods for hyperbolic conservation laws with source terms. Computers & Fluids 23(8), 1049-1071.

Brummer, C.J., Montgomery, D.R., 2003. Downstream coarsening in headwater channels. Water Resources Research 39(10), 1-14.

Caleffi, V., Valiani, A., Bernini, A., 2007. High-order balanced CWENO scheme for movable bed shallow water equations. Advances in Water Resources 30(4), 730-741.

Canestrelli, A., Dumbser, M., Siviglia, A., Toro, E.F., 2010. Well-balanced high-order centered schemes on unstructured meshes for shallow water equations with fixed and mobile bed. Advances in Water Resources 33(3), 291-303.

Cao, Z.X., Li, Y.T., Yue, Z.Y., 2007. Multiple time scales of alluvial rivers carrying suspended sediment and their implications for mathematical modeling. Advances in Water Resources 30(4), 715-729.

Cao, Z.X., Yue, Z.Y., Pender, G., 2011a. Landslide dam failure and flood hydraulics. Part I: experimental investigation. Natural Hazards 59(2), 1003-1019.

Cao, Z.X., Yue, Z.Y., Pender, G., 2011b. Landslide dam failure and flood hydraulics. Part II: coupled mathematical modelling. Natural Hazards 59(2), 1021-1045.

Cartwright J.H.E., Piro, O., 1992. The dynamics of Runge-Kutta methods. International Journal of Bifurcation and Chaos 2(3), 427-449.

Črnjarić-Žic, N., Vuković, S., Sopta, L., 2004. Extension of ENO and WENO schemes to one-dimensional sediment transport equations. Computers & Fluids 33(1), 31-56.

Cui, Y.T., Parker, G., Paola, C., 1996. Numerical simulation of aggradation and downstream fining. Journal of Hydraulic Research 34(2), 185-204.

Cui, Y.T., 2007. The unified gravel-sand (TUGS) model: simulating sediment transport and gravel/sand grain size distributions in gravel-bedded rivers. Water Resources Research 43(10), 1-16.

George, D.L., 2010. Adaptive finite volume methods with well-balanced Riemann solvers for modeling floods in rugged terrain: Application to the Malpasset dam-break flood (France, 1959). International Journal for Numerical Methods in Fluids 66, 1000-1018.

Greenberg, J.M., Leroux, A.Y., 1996. A well-balanced scheme for the numerical processing of source terms in hyperbolic equations. SIAM Journal on Numerical Analysis 33(1), 1-16.

Greimann, B., Lai, Y., Huang, J.C., 2008. Two-dimensional total sediment load model equations. Journal of Hydraulic Engineering 134(8), 1142-1146.

Guo, Q.C., Jin, Y.C., 1999. Modeling sediment transport using depth-averaged and moment equations. Journal of Hydraulic Engineering 125(12), 1262-1269.

Guo, Q.C., Jin, Y.C., 2002. Modeling nonuniform suspended sediment transport in alluvial rivers. Journal of Hydraulic Engineering 128(9), 839-847.

Han, Q.W., 1980. A study on non-equilibrium transport of suspended load. Proc. 1st International Symposium on River Sedimentation, Beijing, China, 793-802.

Hirano, M., 1971. River bed degradation with armouring. Trans. Japan Society of Civil Engineers 195, 55-65(in Japanese).

Hoey, T.B., Ferguson, R., 1994. Numerical simulation of downstream fining by selective transport in gravel bed rivers: model development and illustration. Water Resources Research 30(7), 2251-2260.

Huang, W., 2014. A computational investigation of the dynamic processes of extreme water-sediment hazards. PhD dissertation, Wuhan University, pp. 183 (in Chinese).

Huang, W., Cao, Z.X., Yue, Z.Y., Pender, G., Zhou, J.F., 2012. Coupled modelling of flood due to natural landslide dam breach. Proceedings of the ICE - Water Management 165(10), 525-542.

Komura, S., 1963. Discussion of sediment transportation mechanics: introduction and properties of sediment. Journal of the Hydraulics Division 89(1), 236-266.

Liang, Q.H., Marche, F., 2009. Numerical resolution of well-balanced shallow water equations with complex source terms. Advances in Water Resources 32(6), 873-884.

Parker, G., 1991a. Selective sorting and abrasion of river gravel. I: Theory. Journal of Hydraulic Engineering 117(2), 113-149.

Parker, G., 1991b. Selective sorting and abrasion of river gravel. II: Applications. Journal of Hydraulic Engineering 117(2), 150-171.

Ribberink, J.S., 1987. Mathematical modelling of one-dimensional morphological changes in rivers with non-uniform sediment. Ph.D. thesis, Delft University of Technology, Delft, Netherlands, 206 pp.

Rogers, B.D., Borthwick, A.G.L., Taylor, P.H., 2003. Mathematical balancing of flux gradient and source terms prior to using Roe's approximate Riemann solver. Journal of Computational Physics 192(2), 422-451.

Rosatti, G., Fraccarollo, L., 2006. A well-balanced approach for flows over mobile-bed with high sediment-transport. Journal of Computational Physics 220(1), 312-338.

Seal, R., Paola, C., Parker, G., Southard, J.B., Wilcock, P.R., 1997. Experiments on downstream fining of gravel: I. Narrow-channel runs. Journal of Hydraulic Engineering 123(10), 874-884.

Simpson, G., Castelltort, S., 2006. Coupled model of surface water flow, sediment transport and morphological evolution. Computers & Geosciences 32,1600-1614.

Toro-Escobar, C.M., Paola, C., Parker, G., 1996. Transfer function for the deposition of poorly sorted gravel in response to streambed aggradation. Journal of Hydraulic Research 34(1), 35-53.

Toro, E.F., 2001. Shock-capturing methods for free-surface shallow flows. Wiley, Chichester, UK.

Van Rijn, L.C., 1986. Sediment transport, part III: Bed forms and alluvial roughness. Journal of Hydraulic Engineering 112(6), 433-455.

Venutelli, M., 2002. Stability and accuracy of weighted four-point implicit finite difference schemes for open channel flow. Journal of Hydraulic Engineering 128(3), 281-288.

Viparelli, E., Sequeiros, O.E., Cantelli, A., Wilcock, P.R., Parker, G., 2010. River morphodynamics with creation/consumption of grain size stratigraphy 2: numerical model. Journal of Hydraulic Research 48(6), 727-741.

Wang, Z.G., Bowles, D.S., 2006. Three-dimensional non-cohesive earthen dam breach model. Part 1: Theory and methodology. Advances in Water Resources 29(10), 1528-1545.

Wu, W.M., Wang, S.S.Y., Jia, Y.F., 2000. Nonuniform sediment transport in alluvial rivers. Journal of Hydraulic Research 38(6), 427-434.

Wu, W.M., 2004. Depth-averaged two-dimensional numerical modeling of unsteady flow and nonuniform sediment transport in open channels. Journal of Hydraulic Engineering 130(10), 1013-1024.

Wu, W.M., 2007. Computational River Dynamics. Taylor & Francis Group, London.

Wu, W.M., Wang, S.S.Y., 2006. Formulas for sediment porosity and settling velocity. Journal of Hydraulic Engineering 132(8), 858-862.

Wu, W.M., Wang, S.S.Y., 2008. One-dimensional explicit finite-volume model for sediment transport. Journal of Hydraulic Research 46(1), 87-98.

Xie, J.H. ed. 1990. Mathematical River Modelling. China Water and Power Press, Beijing, China (in Chinese).

Zhang, R.J., Xie, J.H., 1993. Sedimentation research in China-systematic selections. China Water and Power Press, Beijing, China (in Chinese).

Zhou, J.G., Causon, D.M., Mingham, C.G., Ingram, D.M., 2001. The surface gradient method for the treatment of source terms in the shallow-water equations. Journal of Computational Physics 168(1), 1-25.

List of figure captions

Fig. 1 Computed stages and velocities from the WB (a, c) and NWB (b, d) models in static condition at $t = 1$ h (wet bed application)

Fig. 2 Computed stages and velocities from the WB (a, c) and NWB (b, d) models in static condition at $t = 1$ h (with wet-dry interfaces)

Fig. 3 Computed stages and bed profiles at (a) $t = 7.5$ h, and (b) $t = 15$ h from the WB, NWB-CDD and NWB-FDD models along with the measured data for bed

Fig. 4 Computed stages and bed profiles at (a) $t = 7.5$ h, and (b) $t = 15$ h from the WB, NWB-CDD and NWB-FDD models along with the bed profiles computed by Armanini and Di Silvio (1988)

Fig. 5 Sketch of the aggradation experiments (adapted from Seal et al. 1997)

Fig. 6 Computed stages and bed profiles from the WB and NWB models against the measured

Fig. 7 Comparison between the velocity profiles from the WB and NWB models

Fig. 8 Grain size distribution in substrate layer computed by WB model

Fig. 9 Computed characteristic grain sizes in substrate layer from the WB and NWB models compared against the measured

Fig. 10 Computed stage hydrographs from the WB and NWB models against the measured

Fig. 11 Computed water surface and bed profiles from the WB (a1, a2, a3) and NWB (b1, b2, b3) models along with the measured data for stage

Fig. 12 Comparison between the velocity profiles from the WB and NWB models